# Improvements in the Dispersion of Nanosilver in a MgB 2 Matrix through a Graphene Oxide Net

**ARTICLE** *in* THE JOURNAL OF PHYSICAL CHEMISTRY C · MAY 2015

Impact Factor: 4.77 · DOI: 10.1021/jp512165q



**9 AUTHORS**, INCLUDING:

Kaludewa Sujeewa Buddhimali De Silva

University of Technology Sydney

**22** PUBLICATIONS **78** CITATIONS

SEE PROFILE

Jianli Wang

University of Wollongong

**191** PUBLICATIONS **1,279** CITATIONS

SEE PROFILE

Shahriar Hossain

Institute for Superconducting and Electronic…

**63** PUBLICATIONS **589** CITATIONS

SEE PROFILE

J. Horvat

University of Wollongong

**217** PUBLICATIONS **3,882** CITATIONS

SEE PROFILE

THE JOURNAL OF PHYSICAL CHEMISTRY C

Article

pubs.acs.org/JPCC

# Improvements in the Dispersion of Nanosilver in a $MgB_2$ Matrix through a Graphene Oxide Net

Mislav Mustapić,*[,†] Kaludewa S. B. De Silva,[†,‡] Seyed H. Aboutalebi,[†] Shaon Barua,[†] Xun Xu,[†] Jianli Wang,[†] Md. Shariar Hossain,[†] Josip Horvat,[†] and Shi Xue Dou[†]

[†]Institute for Superconducting and Electronic Materials, AIIM, University of Wollongong, Squires Way, North Wollongong, NSW 2500, Australia

[‡]Institute for Nanoscale Technology, Faculty of Science, University of Technology Sydney, City Campus, P.O. Box 123, Broadway, Sydney, NSW 2007, Australia

**ABSTRACT:** The effects of graphene oxide (GO) addition on the dispersion of nanosilver (Ag) in an $MgB_2$ matrix were studied using bulk samples prepared through a diffusion process. The influence of the dispersion of Ag and Ag/GO particles on the critical current density ($J_c$) of $MgB_2$ was also investigated. GO has emerged as an excellent dopant which can significantly improve both the low- and high-field performance of $MgB_2$ due to its capability to improve intergrain connectivity (GO) and inter- and intragrain pinning (GO and AgMg). The addition of nanosize Ag particles also results in an improvement of vortex pinning, and at the same time, it offers the advantage of preventing the loss of Mg during the sintering process. It is found that the dispersion of nanosilver in the presence of GO results in significant improvements in the critical current density in $MgB_2$, particularly at high magnetic fields, due to improved intergrain connectivity and flux pinning. The use of the GO net as a platform for doping $MgB_2$ in our case with Ag yielded a 10-fold-better critical current density ($J_c$) than standard Ag doping at 9 T and 5 K. Even without sophisticated processes, we obtained a $J_c$ result of $10^4$ A/cm$^2$ at 9 T and 5 K, which is one of the best ever achieved.

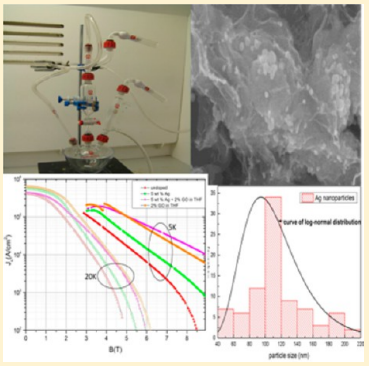

## 1. INTRODUCTION

Since the discovery of superconductivity in $MgB_2$,[1] extensive research has been undertaken to enhance its superconducting properties, such as its critical current density ($J_c$), upper critical field ($H_{c2}$), and irreversibility field ($H_{irr}$). The incorporation of nanosize carbon containing dopants such as SiC, carbon nanotubes (CNT), malic acid, graphene, and graphene oxide into this superconductor has been reported widely as being an effective means of improving the superconducting properties.[2−6] Most carbon dopants, however, have adverse effects on the critical temperature ($T_c$) and the low-field $J_c$ performance. Among these, graphene oxide (GO) has been recognized as an outstanding dopant for $MgB_2$ because of its capability to improve both low- and high-field performance at very low doping levels.[7]

The optimization of the stoichiometry of Mg and B has played a vital role in the fabrication of this superconductor because its microstructure and superconducting properties are greatly affected by the Mg/B ratio.[8] Controlling the Mg/B ratio during sintering is difficult because of the inevitable vaporization of Mg during the sintering process. Usually 20% excess Mg is added to compensate for the Mg loss during the diffusion sintering process. Nanosilver addition has been reported to be an effective sintering aid to facilitate good control during the sintering process. Furthermore, it has been reported that the resultant nanoscale Ag−Mg impurity phases encourage flux pinning resulting in improved superconducting performance at high field.[9,10] The use of nanosilver prepared in-house through chemical synthesis allowed us to incorporate optimized nano-Ag particles into the $MgB_2$ matrix. In this work, we report a significant improvement of $J_c$ in $MgB_2$, with codoping by graphene oxide and nano-Ag.

Previous studies have indicated that GO doped to $MgB_2$ did not show any negative impact on the connectivity of $MgB_2$ grains. Furthermore, recent research shows that GO doping even stimulates the growth of $MgB_2$ grains along preferred crystalline orientations[6,7] and improves the grain connectivity. It was also noticed that layered nanosheets of GO are uniformly spread within and among the $MgB_2$ crystals.[6] This behavior of GO in the $MgB_2$ matrix makes it suitable as a platform for more effective doping of $MgB_2$ by other (previously used) elements and compounds. This produces a synergetic effect of localized atomic (carbon and oxygen) doping and texturing of the crystals (by GO) that significantly enhances both low- and high-field $J_c$. A considerable difference is noticeable between GO doping and doping with other carbon sources, such as graphene or CNT. Doping with graphene and CNT has negative effects on $J_c$ in low magnetic fields due to an increase in disorder in the texturing of $MgB_2$, reducing conductivity between $MgB_2$ grains.[11] Even a small amount of carbon doping (1 wt %) has negative effects on $J_c$ in a low applied magnetic field due to the quick reaction between carbon and boron.

**Received:** December 6, 2014
**Revised:** March 20, 2015





DOI: 10.1021/jp512165q
J. Phys. Chem. C XXXX, XXX, XXX−XXX

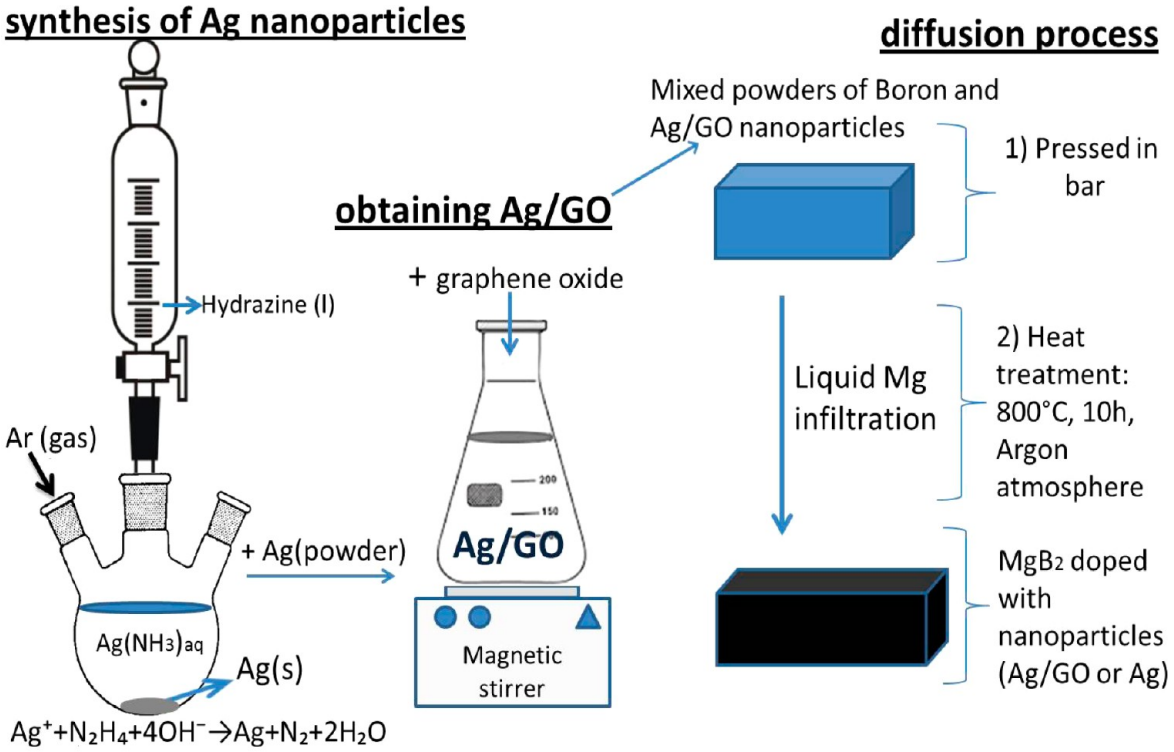


**Figure 1.** Schematic illustration of sample preparation.

The procedure for nano-Ag and GO codoping of $MgB_2$ has been developed in this article. The influence of nano-Ag doping in the presence of GO on the critical temperature, resistivity, grain to-grain connectivity, lattice disorder, and critical fields has also been investigated. The results are compared to those on nondoped samples, and the origin of the difference in the critical current density is discussed. Finally, the effect of the silver nanoparticle dispersion in $MgB_2$ and the following enhancement of $J_c$ is compared to previous research by other groups.

**1.1. Ag Doping by Other Research Groups.** Over the past decade or more, several groups have investigated the influence of Ag doping on $MgB_2$ electromagnetic performance. According to the earliest research, silver doping presents only a small impact on the resistivity characteristic of $MgB_2$. At the same time, many groups have focused on phase formation and the chemistry between elements. The microstructure approach provides vital information about the formation of new phases, temperature dependence, and special distribution of phases during processing. Because it was a promising candidate, some researchers prepared thin films and polycrystals of $MgB_2$ and used different techniques for the preparation of samples, such as high pressure and diffusion methods.

First, Sun et al.[12] in 2002 reported the formation of binary compound $Mg_{0.5}Ag_{0.5}$. Resistivity measurement showed the surprising result that $T_c$ remained close to 39 K even with increased doping by Ag. The $J_c$ results did not show any significant improvement.

In the same year, Zouaoui et al.[13] prepared polycrystalline $MgB_2$ doped with various amounts of Ag. In summary, they demonstrated that $MgB_2$ with a silver admixture shows relatively improved superconducting performance characterized by (a) a slightly higher transition temperature, (b) a lower absolute resistivity in the normal state with a linear $T_c$ dependence, and (c) a higher RRR. Also, they concluded that Ag reacts with excess magnesium and forms intermetallic layers of AgMg that cluster at crystallite boundaries, preventing the formation of $MgB_2$ and inducing disorder in the crystal structure.

Toulemonde et al.[14] investigated the superconducting properties of bulk samples prepared at high applied pressure for several dopant elements (Na, Ca, Cu, Ag, Zn, and Al). Among the above-mentioned dopant elements, Ag doping did not present results worthy of further investigation.

Kumar et al.[15] synthesized silver-doped $MgB_2$ bulk samples. Their report mentions the prevention of Mg loss at higher sintering temperature as well as the formation of pinning centers. Nevertheless, the results of the critical current density obtained in their work showed lower values than the highest reported in the literature.

Song and co-workers[16] doped $MgB_2$ with Ag nanoparticles 30 nm in size and sintered it at the relatively high temperature of 900 °C for 2 h. The XRD results were in agreement with most of those from previous research groups, with the formation of various impurity phases, such as binary compounds MgAg, $MgB_4$, $MgB_6$, and MgO. They reported an enhancement of $J_c$ with Ag doping, and the optimal flux-pinning effect was obtained for 8 wt % Ag. Later, a systematic investigation was carried out by Shekar et al.[9] on the effect of Ag doping on $MgB_2$. By using the same sintering conditions for all doping levels, an optimum $J_c$ was obtained for 10 atom %, which is in good agreement with Song et al. The high value of $J_c$ for the Ag-added $MgB_2$ superconductor was attributed to the inclusion of MgAg nanoparticles (5−20 nm) in the crystal matrix of $MgB_2$.

Kumakura and co-workers[17] were focused on the mechanism of reaction and phase formation related to Ag doping. They reported that the optimal silver addition level for high critical current properties is 2−5% against magnesium, which is a much lower level compared to the eutectic composition of the Mg−


DOI: 10.1021/jp512165q
J. Phys. Chem. C XXXX, XXX, XXX−XXX

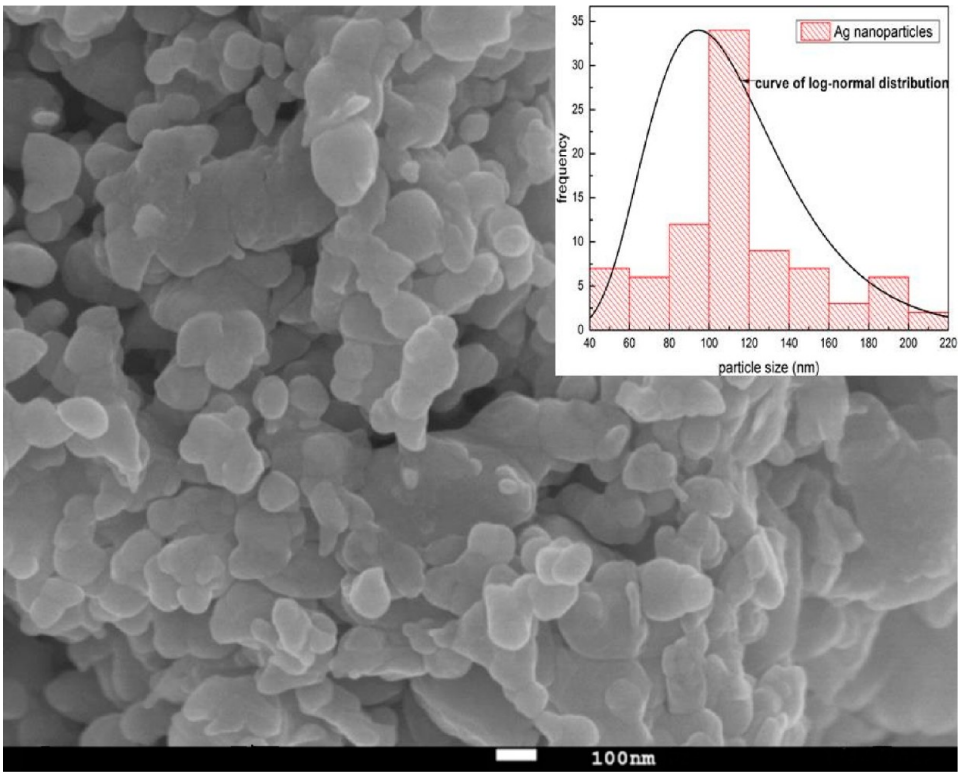


**Figure 2.** SEM image of Ag nanoparticles obtained without the use of surfactants. Inset: the log-normal size distribution obtained from the SEM image.

Ag system. Their research revealed that the synthesis temperature could be lowered to 450 °C by ∼2% silver addition to magnesium, forming a eutectic system. Finally, they concluded that among many candidates for dopants, silver can improve the reactivity of magnesium through decreasing its melting point.

Kimishima et al.[18] mostly investigated $J_c$ of doped $MgB_2$ prepared from a sintered mixture of Mg, B, and $Ag_2O$ in an $H_2$ 10%/Ar atmosphere. They reported Ag−Mg nanoparticles with diameters of 10−15 nm that acted as pinning centers for magnetic flux penetrating $MgB_2$. Their obtained $J_c$ values at 20 K and 1 T were estimated to be $3.2 \times 10^4$, $4.2 \times 10^4$, and $3.6 \times 10^4$ A/cm$^2$ for the $x$ = 0.01 and 0.02 samples, respectively.

Finally, Ranot et al.[19] prepared thin films of $MgB_2$ doped separately with Ag and Cu. They reported a significant enhancement of $J_c$ without the suppression of $T_c$. The increase in $J_c$ resulted from improved grain connectivity and strong flux pinning by the high density of grain boundaries. The Ag doping was more effective than the Cu doping for $J_c$ enhancement in $MgB_2$ films.

All this work indicates the suitability of Ag for the improvement of superconducting properties of $MgB_2$. The use of GO as a means of their dispersion and a potential source of additional carbon doping is investigated in this report.

## 2. EXPERIMENTAL PROCEDURES

**2.1. Sample Preparation.** The sample preparation steps are presented in Figure 1, which are divided into three parts: synthesis of Ag nanoparticles, their attachment to GO sheets, and the preparation of $MgB_2$ by the diffusion method. Silver nanoparticles were synthesized by a wet technique with the chemical reduction of silver salts. Approximately 3.5 mmol of $Ag(NO_3)$ salt was dissolved in 30 mL of deionized (DI) water (Figure 1). In a separate three-necked beaker, 1 mL (31 mmol) of hydrazine was dissolved in 30 mL of DI water, with a few droplets of ethylenediamine to provide an alkaline environment (pH ∼10). In this synthesis, no surfactant was used to prevent repulsion between Ag nanoparticles and GO sheets. Excess reducing agent (10 times greater concentration than silver salt) and an alkaline environment provide the best conditions for the rapid, strong reduction of silver salts.

GO nanosheets were mixed with freshly prepared Ag nanoparticles. The preparation procedure for GO in tetrahydrofuran (THF) solution was reported earlier.[7] This mixture was vigorously stirred for 2 h. Finally, Ag/GO nanoparticles were centrifuged and dried in an oven overnight at 75 °C in a low oxygen atmosphere.

Nondoped and doped bulk $MgB_2$ samples were prepared via the diffusion method. After a systematic study of Ag doping into $MgB_2$,[9,10] 5 wt % nano-Ag was selected as the optimum Ag addition to the $MgB_2$ matrix. The 1 wt % GO doping level was selected as the optimum level for GO doping, based on our previous studies.[7] The codoped sample was prepared through adding these two optimum quantities of Ag and GO, together with the B powder (99.999%, 0.2 to 2.4 $\mu$m in size). Powders were mixed thoroughly using a mortar and pestle and were pressed into pellets 13 mm in diameter. The pellets were inserted into a soft iron tube with Mg powder (99%, 352 mesh) separated from the pellets and in a quantity exceeding (+20%) the stoichiometric ratio of $MgB_2$ to account for its loss during heat treatment. The samples were heat treated at 800 °C for 10 h in a quartz tube at a heating rate of 5 °C min$^{-1}$ under 99.9% pure flowing argon gas.

**2.2. Nanoparticle Characterization.** Figure 2 shows the SEM image of as-prepared Ag nanoparticles, and the inset shows the grain size obtained from SEM images that is


DOI: 10.1021/jp512165q
J. Phys. Chem. C XXXX, XXX, XXX−XXX

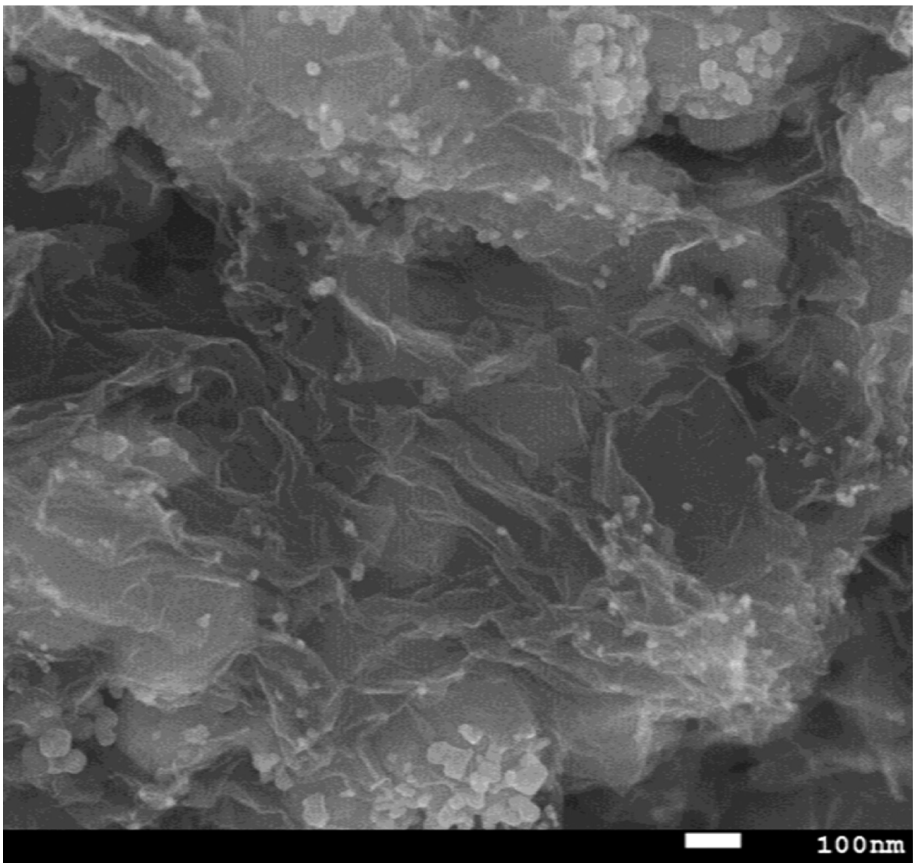


**Figure 3.** SEM image of silver nanoparticles embedded on graphene oxide (GO) sheets. The image shows the dispersion of Ag nanoparticles in the graphene oxide network.

separated into size categories and fitted by log-normal distribution functions. The particle size is broadly distributed, with the smallest particle size at around 30 nm and the largest at around 220 nm. Most of the particles are between 80 and 100 nm in size. Furthermore, the shapes of small particles are mostly spherical, whereas agglomerated particles form irregularly shaped clusters. No surfactants were used for the as-prepared Ag nanoparticles during the preparation reaction, which has a strong effect on the size distribution and shape of the particles. The lack of surfactant promotes an intensified growth of nanoparticles after the nucleation process, mostly by Ostwald ripening.[20]

Scanning electron microscope (SEM), atomic force microscope (AFM), and transmission electron microscope (TEM) characterizations of GO are available in our previous work.[7]

Figure 3 presents sheets of graphene oxide with embedded silver nanoparticles. The GO sheets contain small Ag nanoparticles with a mostly spherical shape as well as agglomerated clusters of silver particles. The smallest nanoparticles are below 50 nm in size, and they are well dispersed into the GO matrix. On the other hand, larger nanoparticles have a tendency to agglomerate in clusters on GO sheets. The clusters occur most likely because of the stronger van der Walls force between the nanoparticles. The GO network partially prevents interaction between particles and thus blocks the agglomerating process upon drying into agglomerated structures (Figure 2). Monolithic graphene is transformed by oxidation into graphene oxide with reactive functional groups such as −OH and −COOH.[21] Silver nanoparticles most likely interact with these groups because of electrostatic interaction and are pinned onto the graphene oxide net.

The XRD pattern of the Ag nanoparticles (Figure 4) shows that Ag nanoparticles of high purity were synthesized, with observed peaks at 38.10, 44.09, and 64.36° (JCPDS, file no. 4-0783). On the other hand, the XRD pattern of Ag/GO shows identical peaks of Ag, with substantially more noise and two amorphous halos in the region between 10 and 20°, which may

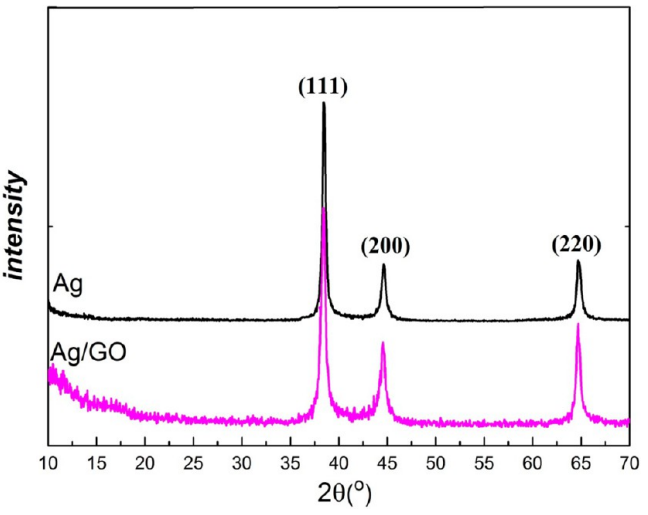


**Figure 4.** XRD patterns of Ag nanoparticles and Ag/GO.



DOI: 10.1021/jp512165q
J. Phys. Chem. C XXXX, XXX, XXX−XXX

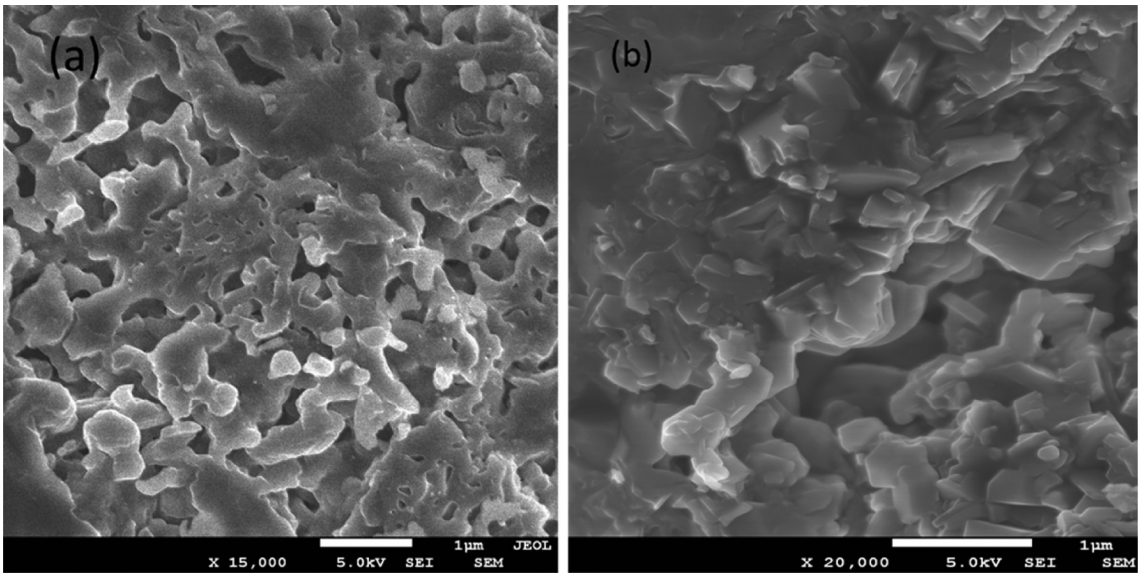


**Figure 5.** SEM image of (a) nondoped $MgB_2$ and (b) $MgB_2$ doped with Ag/GO.

indicate the presence of amorphous carbon.[22] There is no shifting of peaks observed between two patterns.

**2.3. $MgB_2$ Characterization.** The phase identification and crystal structure investigations were carried out using an X-ray diffractometer (GBCMMA) with Cu K$\alpha$ radiation ($\lambda$ = 1.54059 Å). A JEOL JSM-7500FA field emission scanning electron microscope (FESEM) was used for SEM analysis. The superconducting transition temperature, $T_c$, was determined from the magnetic ac susceptibility measurements, and the magnetic $J_c$ was derived from the width of the magnetization loop using the modified Bean model.[23] The hysteresis loops were measured with a quantum design physical properties measurement system (PPMS). The resistivity measurements were conducted using the standard dc four-probe technique under magnetic fields of up to 13 T in the PPMS. The upper critical field ($H_{c2}$) and the irreversibility field ($H_{irr}$) were determined using the 90 and 10% criteria of $R$(40 K) for different applied fields, where $R$(40 K) is the normal state resistance in the vicinity of 40 K. The active cross-section ($A_F$) was calculated from the resistivity, $\rho$, by Rowell's method.[24]

## 3. RESULTS AND DISCUSSION

Figure 5a,b shows secondary electron images taken by FESEM of pure and Ag/GO-doped $MgB_2$, respectively. The images indicate a rather homogeneous $MgB_2$ grain structure, with an apparent grain size of around 200 nm. It gives visible evidence of the improved intergrain connectivity in the doped sample because the doped sample appears to be denser and to have well-connected grains compared to the nondoped sample.

The XRD measurements were performed on ground $MgB_2$ pellets. According to the Rietveld analysis of undoped $MgB_2$ (Figure 6a), all peaks marked with Miller indices belong to the pure $MgB_2$ phase, without any other common phase as a MgO or unreacted Mg. The GO-doped sample (Figure 6b), besides distinguished $MgB_2$ peaks, shows unreacted Mg peaks in a relatively small amount. It is interesting that the MgO phase has not been detected, indicating the preservation of most GO layers between $MgB_2$ grains.[6] This is consistent with the appearance of unreacted magnesium, which usually reacts with oxygen to give MgO.

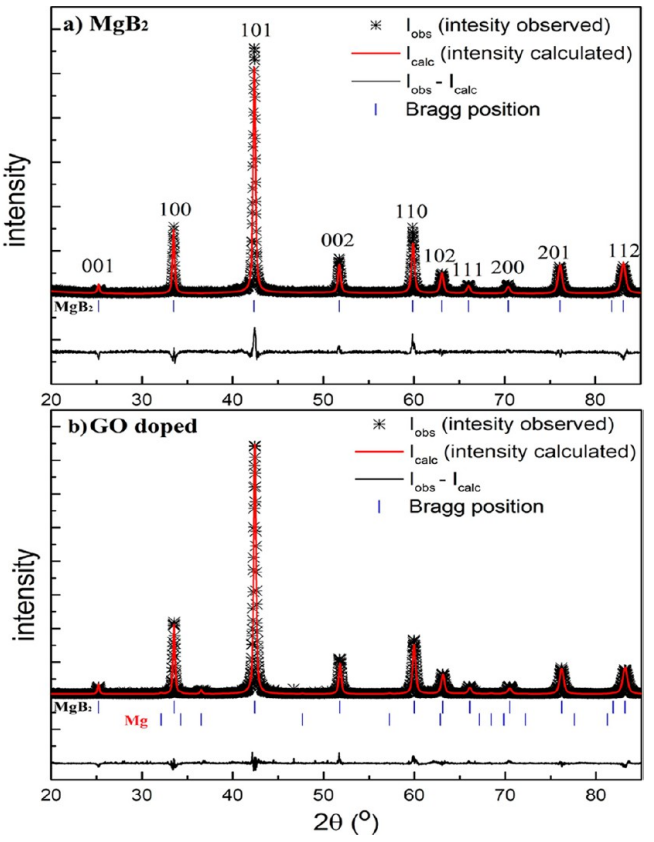


**Figure 6.** Fitting of the XRD pattern in Rietveld refinement for pure $MgB_2$ (a) and GO-doped $MgB_2$ (b). The positions of $MgB_2$ and Mg peaks are shown in the first and second (b) rows below the XRD patterns, respectively. An enlarged difference between the experimental XRD pattern and our fit to this pattern is shown in the bottom row.

Doping with nano-Ag (Figure 7a), however, has resulted in additional peaks at angles of 26.88, 38.40, 47.51, 55.50, 62.6, and 69.30°, revealing the second phase as AgMg (ICDD card no. 00-029-0871) in the $MgB_2$ matrix. Similarly, Zouaoui et al.[13] have reported the presence of the same MgAg phase


DOI: 10.1021/jp512165q
J. Phys. Chem. C XXXX, XXX, XXX−XXX

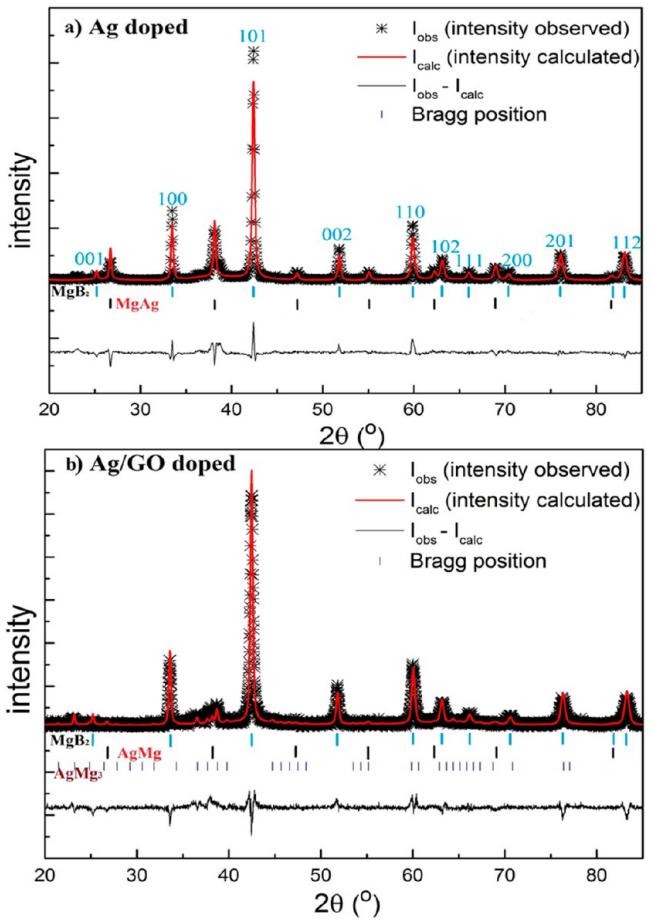


**Figure 7.** Fitting of the XRD pattern in the Rietveld refinement for Ag-doped $MgB_2$ (a) and Ag/GO-doped $MgB_2$ (b). The positions of $MgB_2$, AgMg, and $AgMg_3$ peaks are shown in the first, second, and third rows below the XRD patterns, respectively. The enlarged difference between the experimental XRD pattern and our fit to this pattern is shown in the bottom row.

(ICDD card no. 00-029-0871), as well as Ag and unreacted Mg in the XRD analysis of $MgB_2$ doped with Ag (2, 6, and 16 wt %). It is important to notice that unreacted Mg, Ag, or MgO has not been detected in Ag-doped samples.

On the other hand, the Ag/GO pattern (Figure 7b) presents the most complex phase composition with a substantial percentage of the $AgMg_3$ phase (ICDD card no. 00-001-1170) and a lower percentage of the AgMg phase. Beside the two mentioned new phases, pure $MgB_2$ was mostly detected. Kumar et al.[15] also noticed the $AgMg_3$ phase and described it as crucial pinning centers responsible for obtaining high $J_c$. The key difference between Ag and Ag/GO doping, and consequently $J_c$ results, was the different percentages of the AgMg and $AgMg_3$ intermetallic phases. According to the literature,[25] the formation mechanism of these phases is a peritectic reaction during the cooling process. The formation of $AgMg_3$ is related to the peritectic reaction and occurs in a very narrow part of the Ag−Mg phase diagram at $X_{Mg}$ = 0.75−0.80, during the slow cooling process (liquid + MgAg ↔ $AgMg_3$).

The explanation of the difference in phase formation between two samples can be the GO layers. Graphene oxide sheets seem to cover silver nanoparticles, as indicated in Figure 3, impeding the direct reaction between Mg and Ag. Because of that, a larger concentration of magnesium infiltrating boron + nanoparticles pellets is needed to penetrate the dense GO sheets and react with Ag in a more significant amount than without GO. After the sintering period, during the natural cooling process, a higher concentration of Mg ($X_{Mg}$ > 0.70) promotes the peristaltic reaction and the formation of the $AgMg_3$ phase. Furthermore, Rietveld refinement was done using the FullProf software package to determine the lattice parameters of the $MgB_2$ phase. Lattice parameters *a* and *c*, the fwhm, and the microstrain of all samples are given in Table 1. Lattice parameters *a* and *c* show a decreasing trend with doping.

**Table 1. Lattice Constants *a*, *c*, and *c*/*a* and Strain of Pure $MgB_2$, 5 wt % Ag-Doped $MgB_2$, 2 wt % GO-Doped $MgB_2$, and 5 wt % Ag- + 2 wt % GO-Doped $MgB_2$**

| | lattice parameter (Å) Rietveld refinement | | | |
|---|---|---|---|---|
| sample | *a* | *c* | *c*/*a* | strain (W−H plot) (%) |
| $MgB_2$ | 3.08873 | 3.53126 | 1.1433 | 0.1313 |
| $MgB_2$ + 5 wt % Ag | 3.08859 | 3.52882 | 1.1425 | 0.1537 |
| $MgB_2$ + 2 wt % GO | 3.08473 | 3.52911 | 1.1440 | 0.1889 |
| $MgB_2$ + 5 wt % Ag + 2 wt % GO | 3.08087 | 3.52892 | 1.1454 | 0.2194 |

Rietveld refinement also provided phase distribution data (Figures 6 and 7), so for the 2 wt % GO doped sample we have a 99.1 wt % $MgB_2$ phase and 0.9 wt % unreacted Mg. The Ag-doped sample contains 95.2 wt % pure $MgB_2$, 4.7 wt % AgMg, and 0.1 wt % $AgMg_3$. On the other hand, the Ag/GO codoped sample has a 96.5 wt % $MgB_2$ phase, a 0.5 wt % AgMg phase, and a 3.0 wt % $AgMg_3$ phase.

Figure 8a,b shows a substantial shift of the 002 and 110 diffraction peaks toward higher angles, which indicates carbon

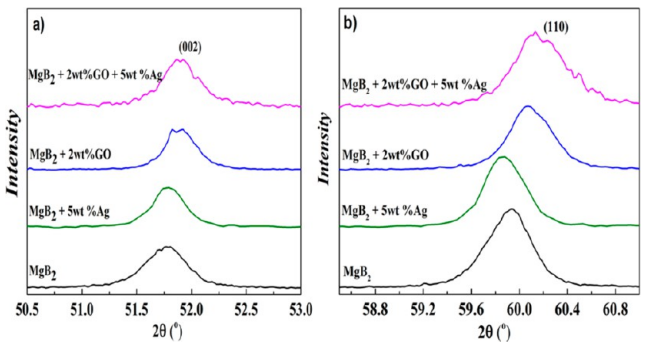


**Figure 8.** (a, b) Shifting of (002) and (110) peaks with GO and Ag/GO doping.

substitution into the $MgB_2$ crystallites (commonly known to improve intragrain pinning[5−7]) for GO- and Ag/GO-doped samples. The approximate amount of carbon substitution for boron in $MgB_2$ can be obtained from the variation of crystal lattice parameter *a* using a calibration given in Lee et al.[26] Describing the C substitution by $Mg(B_{1-x}C_x)_2$, we obtained $x$ = 0.0125 for GO-doped and $x$ = 0.025 for Ag/Go-doped samples. The obtained results indicate a low level of boron substitution by carbon.

The phase shifting observed for GO and Ag/GO doping is in good agreement with the study of Sudesh et al.,[27] where phase shifting and strain have been increased with increasing GO


DOI: 10.1021/jp512165q
J. Phys. Chem. C XXXX, XXX, XXX−XXX

doping from 1 to 10 wt %. On the other hand, Ag-doped samples did not show any shifting of the 110 and 220 reflections of $MgB_2$, which indicates that the AgMg phase is concentrated between $MgB_2$ grains (Figure 8a,b).

Yeoh et al.[6] have performed 3D atom probe tomography for GO-doped samples and presented a precise distribution of carbon and oxygen atoms as well as the location of individual GO platelets. Their study shows that GO layers are uniformly dispersed in the $MgB_2$ matrix. Furthermore, the partial segregation of carbon and oxygen (from GO layers) has been observed, which finally enables the replacment of boron with carbon and causes phase shifting.

The microstrain analysis was performed with the Williamson–Hall plot. From this plot, the crystallite size and strain can be extracted from the *y* intercept and gradient of the linear fit to the experimental data, respectively (Table 1, Figure 9).[28] The data was corrected for instrumental broadening using the XRD pattern of the silicone standard sample.

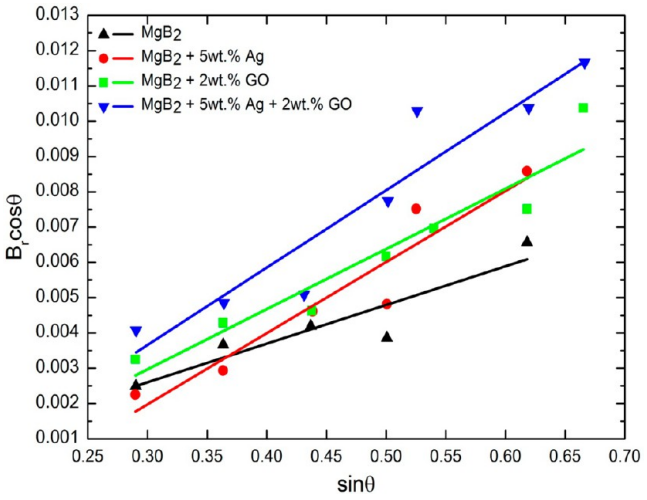


**Figure 9.** Williamson–Hall plot[28] to determine lattice strain for pure $MgB_2$, 5 wt % Ag-doped $MgB_2$, 2 wt % GO doped-doped $MgB_2$, and 5 wt % Ag- + 2 wt % GO-doped $MgB_2$.

The obtained results show the increase in strain for all doped samples, with obtained strain results given in Table 1 for all samples. These results are in good agreement with the strain calculation of pure $MgB_2$ and GO-doped $MgB_2$ in ours previous work.[7] We could not obtain reliable values for the change in crystallite size with doping with this method, due to data scattering.

DTA was performed on mixed powders pressed in small bars (~200 mg) for Mg, B and Ag/GO and Ag nanoparticles, which were pressed and placed in an $Al_2O_3$ pan. Samples were measured as the temperature was increased up to 1000 °C at a rate of 5 K $min^{-1}$ in an inert atmosphere of argon gas.

DTA curves (Figure 10) show similarity with previous research on samples doped with Ni–Co–B nanoparticles.[29−31] All three observed curves have standard peaks associated with the melting of magnesium at 650 °C and the formation of $MgB_2$ at 750 °C. Doped samples have an additional peak at 480 °C that is related to the formation of a eutectic system between Ag nanoparticles and magnesium. According to the Ag–Mg phase diagram, the Ag–Mg phase is dominant in the range of 30–80 atom % magnesium and up to a temperature of 820 °C, whereas in a narrow phase range ($X_{Mg}$ > 75–80%) the

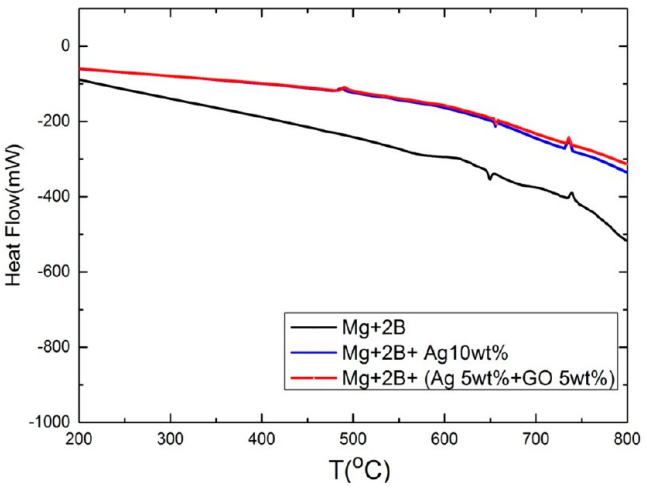


**Figure 10.** DTA curve of mixed powders of Mg + 2B (bottom), Mg + 2B + Ag 10 wt % (middle), and Mg + 2B + (Ag 5 wt % + GO 5 wt %) (top).

formation of $AgMg_3$ has occurred up to a temperature of 469 °C.[25,32]

The creation of this type of Mg–Ag compound strongly depends on the particular composition and percentages of elements especially for nanosized materials. The formation of the eutectic system has been reported for many other types of nanoparticle doping.[29,33,34] It is important to note that in the preparation of samples for DTA analysis all starting materials are premixed together and measured. This is quite different than the diffusion method where just boron and nanoparticles are mixed together and pressed into a bar, whereas liquid magnesium starts to infiltrate the premixed bar at ≤650 °C. Finally, in the diffusion technique of $MgB_2$ growth, the creation of a $MgAg_3$ phase can occur only by a cooling process in the peritectic reaction.

Table 2 presents the critical temperature, the resistivity at 300 and 40 K, the residual resistivity ratio (RRR), and the active cross-sectional area ($A_F$) of the nondoped, nano-Ag-doped, GO-doped, and codoped $MgB_2$ bulk samples. Considerable $T_c$ degradation[35] and the presence of impurity phases[36] can be observed. It is worth noting, however, that the reduction of $T_c$ due to nano-Ag addition is low compared to carbon dopants at the same level of doping.[2−4] The samples doped with 5 wt % nano-Ag and 2 wt % GO showed low resistivity values; however, the codoped samples showed a much higher resistivity value. The presence of impurity phases and the substitution of carbon onto boron sites are believed to be responsible for the increase in the resistivity in the codoped sample. Because Ag nanoparticles were dispersed evenly through the sample due to the presence of GO (Figure 1), these nanoparticles may have introduced a strain field into $MgB_2$ grains throughout the sample. This would then result in the observed increased resistivity of Ag/GO codoped $MgB_2$. The smaller observed $A_F$ compared to that for GO-doped $MgB_2$ is consistent with this picture (Table 2), as Ag nanoparticles also cause local grain misalignment. On the basis of our previous work, GO seems to provide a platform for the uniform nucleation of $MgB_2$ grains, which has resulted in a remarkable improvement in the intergrain connectivity with a higher active cross-section area ($A_F$).[6] GO doping does not result in increased resistivity due to interband and intraband scattering, which would be expected for carbon doping.[8] The lower-than-


DOI: 10.1021/jp512165q
J. Phys. Chem. C XXXX, XXX, XXX–XXX

Table 2. Critical Temperature ($T_c$), Resistivity at 300 and 40 K, Residual Resistivity Ratio (RRR), Active Cross-Section ($A_F$), Upper Critical Field ($H_{c2}$), and Irreversibility Field ($H_{irr}$) of Nondoped, Ag-Doped, GO-Doped, and Ag + GO Codoped Bulk Samples

| sample | $T_c$ (K) | $\rho$(300 K) ($\mu\Omega$ cm) | $\rho$(40K) ($\mu\Omega$ cm) | RRR ($\mu\Omega$ cm) | $A_F$ (%) | $H_{c2}$ at 25 K (T) | $H_{irr}$ at 25 K (T) |
|---|---|---|---|---|---|---|---|
| nondoped $MgB_2$ | 38.9 | 47.02 | 12.74 | 3.69 | 21.4 | 9.4 | 7.6 |
| $MgB_2$ + 5 wt % Ag | 38.15 | 35.87 | 10.26 | 3.5 | 28.0 | 9.4 | 7.6 |
| $MgB_2$ + 2 wt % GO | 37.7 | 21.4 | 9.08 | 2.36 | 59.0 | 11.1 | 8.5 |
| $MgB_2$ + 5 wt % Ag + 2 wt % GO | 36.3 | 61.57 | 32.71 | 1.88 | 25.0 | 12.4 | 9.1 |

expected resistivity of the GO-doped sample occurs because of the prevailing effect of improved grain connectivity. GO was dispersed evenly through the $MgB_2$ sample, producing no agglomerates that would disturb the $MgB_2$ grain connectivity.

The residual resistivity ratio (RRR) gives an indication of the disorder in the sample, so the decreased RRR values compared to those of the nondoped sample reflect the influence of doping on increasing the defects in $MgB_2$ crystals.[36] The addition of Ag nanoparticles decreased the RRR value very little, indicating that the Ag nanoparticles did not disperse enough to produce substantial defects in the $MgB_2$ crystals. This was expected because no surfactants were used for the nanoparticles and they lumped together. GO doping decreased RRR by about 35%, introducing the defects through carbon substitution.[2−7,26] GO + Ag codoping decreases the value of RRR by about 50%. Ag nanoparticles were dispersed on GO sheets, making them much more effective in the creation of defects, in addition to the defects introduced by the C released from the surface of GO sheets. A strongly increased value of resistivity with codoping is consistent with the strongly decreased value of RRR. This also correlates well with the observed higher $H_{c2}$ and $H_{irr}$ values of the codoped samples compared to those of the nondoped and other doped samples, owing to higher intraband impurity scattering due to defects introduced by codoping.

Figure 11 shows the field dependence of $J_c$ of the pure $MgB_2$ and Ag-doped samples at 5 and 20 K. In this particular research,

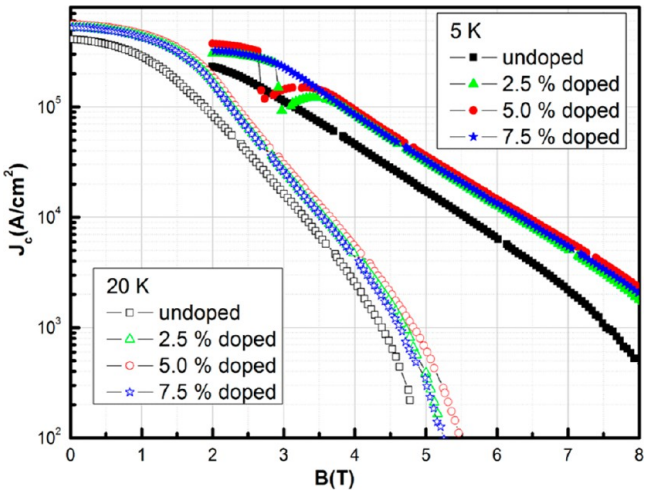


Figure 11. Field dependence of the critical current density of pure and Ag-doped samples.

the optimization of doping with Ag nanoparticles was conducted, with doping at 2.5, 5, and 7.5 wt %. All three doped samples showed an improvement in the critical current density in comparison to that of the pure sample, but with small differences among themselves. Among the doped samples, 5 wt % Ag doping gives the largest value of $J_c$, measured at both 5 and 20 K. The present values of $J_c$ are in the range of common results for samples doped with silver.

Figure 12 shows the in-field $J_c$ performance at 5 and 20 K for nondoped, nano-Ag doped, GO-doped, and nano-Ag/GO

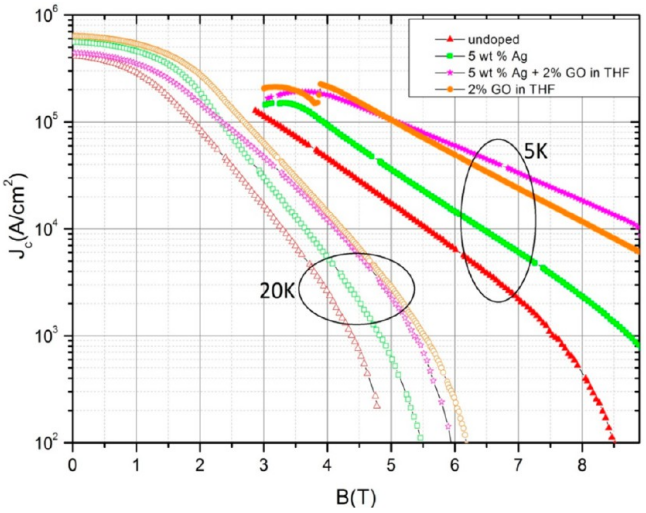


Figure 12. Field dependence of the critical current density obtained for pure $MgB_2$ and the Ag-doped, GO-doped, and Ag/GO-codoped $MgB_2$ samples.

codoped bulk samples of $MgB_2$. The $J_c$ curves for the doped and codoped samples show a significant improvement over those of the nondoped sample at both 5 and 20 K. The sample with 1 wt % GO showed a $J_c$ of 6.35 × $10^5$ A/cm$^{-2}$ at 20 K under zero field. As reported by Wang et al.,[37] a strong correlation exists between the connectivity and the self-field $J_c$, so better grain connectivity and higher $A_F$ values gives higher self-field $J_c$ values. On the other hand, high-field $J_c$ performance is mainly governed by $H_{c2}$ and the flux pinning.[38] The sample codoped with nano-Ag and GO shows a remarkable value of $J_c$, 6.08 × $10^4$ A/cm$^2$ at 5 K, 8 T, which is comparable to the highest $J_c$ ever reported for bulk $MgB_2$ samples. Some level of carbon substitution on boron sites and the presence of a nanosize $AgMg_3$ impurity phase have significantly improved $J_c$ at high fields, through enhanced $H_{c2}$ and flux pinning. As can be seen, the Ag/GO-doped sample has a lower value of $J_c$ at low magnetic field than the GO-doped sample because it has considerably more impurities (Ag + GO).

## 4. CONCLUSIONS

In this work we present a systematic study of the effects of Ag and GO codoping on the critical current density, crystallinity, and resistivity of $MgB_2$ bulk samples. The GO/Ag codoping remarkably improved $J_c$ properties under high fields and enhanced the critical fields. The obtained results are among the best achieved for any doped $MgB_2$ samples. Ag/GO codoping


DOI: 10.1021/jp512165q
J. Phys. Chem. C XXXX, XXX, XXX−XXX

has several advantages. GO helps disperse as-prepared Ag nanoparticles in $MgB_2$ so that Ag nanoparticles homogeneously react with Mg and create effective pinning centers of $AgMg_3$ and AgMg in $MgB_2$ while not having significant deleterious effect on grain connectivity. The formation of the $AgMg_3$ phase (for Ag/GO codoped $MgB_2$) is a crucial factor in the improvement of vortex pinning in $MgB_2$, especially enhancing superconducting performance at high magnetic fields.

On the other hand, GO promotes the alignment of $MgB_2$, improving the grain connectivity. Carbon from GO seems to be incorporated into $MgB_2$ (replacing boron), additionally improving vortex pinning. Furthermore, the AgMg phase was significantly present with Ag doping, but with considerably less effect on the flux pinning in comparison to Ag/GO codoping.

The diffusion method provides maximal efficient reactivity of magnesium through samples with fewer vacancies caused by melting magnesium than for in-situ-prepared samples, providing denser samples with better connectivity among grains. GO net provides a uniform dispersion of doped materials. In comparison to previous research by other groups, Ag/GO codoping significantly improves the critical current results, especially at high magnetic field, shifting the limits of $MgB_2$ applications.

## AUTHOR INFORMATION


### Corresponding Author

*E-mail: mislav@uow.edu.au.


### Notes

The authors declare no competing financial interest.

## ACKNOWLEDGMENTS

This research was performed with the support of the Australian Research Council (ARC) through Project LP0989352 and Hyper Tech Research Inc., USA. We thank P. Hayes, K. Konstantinov, and M. B. Cortie for their helpful discussions. We also thank Dr. Tania Silver for critically reading the article.

## REFERENCES


(1) Nagamatsu, J.; Nakagawa, N.; Muranaka, T.; Zenitani, Y.; Akimitsu, J. Superconductivity at 39 K in Magnesium Diboride. *Nature* **2001**, *410*, 63−64.

(2) Yeoh, W. K.; Kim, J. H.; Horvat, J.; Dou, S. X.; Munroe, P. Improving Flux Pinning of $MgB_2$ by Carbon Nanotube Doping and Ultrasonication. *Supercond. Sci. Technol.* **2006**, *20*, 5.

(3) Dou, S. X.; Shcherbakova, O.; Yeoh, W. K.; Kim, J. H.; Soltanian, S.; Wang, X. L.; Senatore, C.; Flukiger, R.; Dhalle, M.; Husnjak, O.; Babic, E. Mechanism of Enhancement in Elektromagnetic Properties of $MgB_2$ by Nano SiC Doping. *Phys. Rev. Lett.* **2007**, *98*, 097002.

(4) Kim, J. H.; Zhou, S.; Hossain, M. S. A.; Pan, A. V.; Dou, S. X. Carbohydrate Doping to Enhance Electromagnetic Properties of $MgB_2$ Superconductors. *Appl. Phys. Lett.* **2006**, *89*, 142505−3.

(5) Xu, X.; Dou, S. X.; Wang, X. L.; Kim, J. H.; Choucair, M.; Yeoh, W. K.; Zheng, R. K.; Ringer, S. P. Graphene Doping to Enhance the Flux Pinning and Supercurrent Carrying Ability of a Magnesium Diboride Superconductor. *Supercond. Sci. Technol.* **2010**, *23*, 085003.

(6) Yeoh, W. K.; Cui, X. Y.; Gault, B.; De Silva, K. S. B.; Xu, X.; Liu, H. W.; Yen, H. W.; Wong, D.; Bao, P.; Larson, D. J.; et al. On the Roles of Graphene Oxide Doping for Enhanced Supercurrent in $MgB_2$ Based Superconductors. *Nanoscale* **2014**, *6*, 6166−6172.

(7) De Silva, K. S. B.; Aboutalebi, S. H.; Xu, X.; Wang, X. L.; Li, W. X.; Konstantinov, K.; Dou, S. X. A Significant Improvement in Both Low- and High-Field Performance of $MgB_2$ Superconductors Through Graphene Oxide Doping. *Scr. Mater.* **2013**, *69*, 437−440.

(8) Zhang, Y.; Dou, S. X.; Lu, C.; Zhou, S. H.; Li, W. X. Effect of Mg/B Ratio on the Superconductivity of $MgB_2$ Bulk with SiC Addition. *Phys. Rev. B* **2010**, *81*, 094501.

(9) Shekhar, C.; Giri, R.; Tiwari, R. S.; Srivastava, O. N.; Malik, S. K. High Critical Current Density and Improved Flux pinning in Bulk $MgB_2$ Synthesized by Ag Addition. *J. Appl. Phys.* **2007**, *101*, 043906−043906−6.

(10) Grivel, J. C.; Abrahamsen, A.; Bednarčík, J. Effects of Cu or Ag Additions on the Kinetics of $MgB_2$ Phase Formation in Fe-Sheathed Wires. *Supercond. Sci. Technol.* **2008**, *21*, 035006.

(11) Xu, X.; Dou, S. X.; Wang, X. L.; Kim, J. H.; Stride, J. A.; Choucair, M.; Yeoh, W. K.; Zheng, R. K.; Ringer, S. P. Graphene Doping to Enhance the Flux Pinning and Supercurrent Carrying Ability of a Magnesium Diboride Superconductor. *Supercond. Sci. Technol.* **2010**, *23*, 085003.

(12) Sun, T.; Zhang, X. P.; Zhao, Y. G.; Shen, R.; Wang, K.; Zhang, L. W.; Cao, B. S.; Xiong, Y. H.; Li, P. J.; Wen, H. H. Study of the Reactions Between $MgB_2$ and Ag at High Temperature. *Physica C* **2002**, *382*, 367.

(13) Zouaoui, M.; M'chirgui, A.; Ben, A. F.; Yangui, B.; Ben, S. M. Electron Transport Properties of Silver Added Polycrystalline $MgB_2$. *Physica C* **2002**, *382*, 217−223.

(14) Toulemonde, P.; Musolino, N.; Flukiger, R. High-Pressure Synthesis of Pure and Doped Superconducting $MgB_2$ Compounds. *Supercond. Sci. Technol.* **2003**, *16*, 231.

(15) Kumar, D.; Pennycook, S. J.; Narayan, J.; Wang, H.; Tiwari, A. Role of Silver Addition in the Synthesis of High Critical Current Density $MgB_2$ Bulk Superconductors. *Supercond. Sci. Technol.* **2003**, *16*, 455−458.

(16) Song, K. J.; Kim, S. W.; Park, C.; Chung, J. K.; Yang, J. S.; Joo, J. H.; Ko, R. K.; Ha, H. S.; Kim, H. S.; Ha, D. W.; et al. The Effect of Nano-Powder Additions on the Superconducting Properties of $MgB_2$. *IEEE Trans. Appl. Supercond.* **2005**, *15*, 3288.

(17) Shimoyama, J.; Hanafusa, K.; Yamamoto, A.; Katsura, Y.; Horii, S.; Kishio, K.; Kumakura, H. Catalytic Effect of Silver Addition on the Low Temperature Phase Formation of $MgB_2$. *Supercond. Sci. Technol.* **2007**, *20*, 307−311.

(18) Kimishima, Y.; Takami, S.; Uehara, M.; Numa, S.; Sugiyama, Y.; Kuramoto, T. Pinning Properties of Ag/$MgB_2$ Bulk System. *Physica C* **2008**, *468*, 1181−1184.

(19) Ranot, M.; Seong, W. K.; Jung, S.-G.; Lee, N. H.; Kang, W. N.; Joo, J. H.; Zhao, Y.; Dou, S. X. Enhancement of the Critical Current Density of $MgB_2$ Thick Films by Ag-and Cu-Impurity Layers. *Physica C* **2009**, *469*, 1563−1566.

(20) Ostwald, W. Lehrbuck der Allgemeinen Chemie. *Z. Anorg. Chem.* **1897**, *15*, 239.

(21) Sun, L.; Fugetsu, B. Mass Production of Graphene Oxide from Expanded Graphite. *Mater. Lett.* **2013**, *109*, 207−210.

(22) Cui, P.; Lee, J.; Hwang, E.; Lee, H. One-Pot Reduction of Graphene Oxide at Subzero Temperatures. *Chem. Commun.* **2011**, *47*, 12370−12372.

(23) Bean, C. P. Magnetization of High-Field Superconductors. *Rev. Mod. Phys.* **1964**, *36*, 31−39.

(24) Rowell, J. M. The Widely Variable Resistivity of $MgB_2$ Samples. *Supercond. Sci. Technol.* **2003**, *16*, R17.

(25) Cahn, R. W., Haasen, P., Eds.; *Physical Metallurgy*, 4th ed.; North-Holland: Amsterdam, 1996; Vol. *1*, p 492.

(26) Lee, S.; Masui, T.; Yamamoto, A.; Hiroshi, U. H.; Tajima, S. Carbon-Substituted $MgB_2$ Single Crystals. *Physica C* **2003**, *397*, 7−13.

(27) Sudesh; Kumar, N.; Das, S.; Bernhard, C.; Varma, G. D. Effect of Graphene Oxide Doping on Superconducting Properties of Bulk $MgB_2$. *Supercond. Sci. Technol.* **2013**, *26*, 095008.

(28) Williamson, G. K.; Hall, W. H. X-ray Line Broadening from Filed Aluminium and Wolfram. *Acta Metal.* **1953**, *1*, 22−31.

(29) Mustapić, M.; Horvat, J.; Hossain, M. S.; Skoko, Ž.; Sun, Z.; Mitchell, D. R. G.; Dou, S. X. Novel Synthesis of Superparamagnetic Ni−Co−B Nanoparticles and Their Effect on Superconductor Properties of $MgB_2$. *Acta Mater.* **2014**, *70*, 298−306.




DOI: 10.1021/jp512165q
J. Phys. Chem. C XXXX, XXX, XXX−XXX

(30) Mustapić, M.; Horvat, J.; Hossain, M. S.; Skoko, Ž.; Dou, S. X. Interplay Between Boron Precursors and Ni-Co-B Nanoparticles Doping in the Fabrication of $MgB_2$ Superconductor with Improved Electromagnetic Properties. *Acta Mater.* **2014**, *80*, 457−467.
(31) Mustapić, M.; Horvat, J.; Hossain, M. S.; Skoko, Ž.; Dou, S. X. Enhancing Superconducting Properties of $MgB_2$ Pellets by Addition of Amorphous Magnetic Ni−Co−B nanoparticles. *Supercond. Sci. Technol.* **2013**, *26*, 075013.
(32) Zemczuznyj, S. F. On the Alloys of Magnesium with Silver. *Z. Anorg. Chem.* **1906**, *49*, 400−414.
(33) Chen, S. K.; Lockman, Z.; Wei, M.; Glowacki, B. A.; MacManus-Driscoll, J. L. Improved Current Densities in $MgB_2$ by Liquid-Assisted Sintering. *Appl. Phys. Lett.* **2005**, *86*, 242501.
(34) Grivel, J.-C.; Andersen, N. H.; Pallewatta, P. G. A. P.; Zhao, Y.; Zimmermann, M. Influence of Bi, Se and Te Additions on the Formation Temperature of $MgB_2$. *Supercond. Sci. Technol.* **2012**, *25*, 015010.
(35) Teruo, M.; Kiuchi, M.; Yamamoto, A.; Shimoyama, J.; Kohji, K. Essential Factors for the Critical Current Density in Superconducting $MgB_2$: Connectivity and Flux Pinning by Grain Boundaries. *Supercond. Sci. Technol.* **2008**, *21*, 015008.
(36) Wilke, R. H. T.; Budko, S. L.; Canfield, P. C.; Finnemore, D. K.; Suplinskas, R. J.; Hannahs, S. T. Systematic Effects of Carbon Doping on the Superconducting Properties of $Mg(B_{1x}C_x)_2$. *Phys. Rev. Lett.* **2004**, *92*, 217003.
(37) Wang, X.-L.; Dou, S. X.; Hossain, M. S. A.; Cheng, Z. X.; Liao, X. Z.; Ghorbani, S. R.; Yao, Q. W.; Kim, J. H.; Silver, T. Enhancement of the In-Field $J_c$ of $MgB_2$ via $SiCl_4$ Doping. *Phys. Rev. B* **2010**, *81*, 224514.
(38) Li, W. X.; Li, Y.; Chen, R. H.; Zeng, R.; Dou, S. X.; Zhu, M. Y.; Jin, H. M. Raman Study of Element Doping Effects on the Superconductivity of $MgB_2$. *Phys. Rev. B* **2008**, *77*, 094517.


DOI: 10.1021/jp512165q
*J. Phys. Chem. C* XXXX, XXX, XXX−XXX